THE ROLE OF MICROCRACKING ON THE CRACK GROWTH RESISTANCE OF BRITTLE SOLIDS AND COMPOSITES

S. B. Biner

Ames Laboratory
Iowa State University
Ames, Iowa 50011 U.S.A

Abstract

A set of numerical analyses of crack growth was preformed to elucidate the influence of microcracking on the fracture behavior of microcracking brittle solids and composites. The random nucleation, orientation and size effects of discrete nucleating microcracks and resulting interactions are fully accounted for in a hybrid finite element model. The results obtained from the finite element analysis are compared with the continuum description of the microcracking. Although continuum description can provide a reasonable estimation of shielding, it fails to resolve the details of micromechanism of toughening resulting from microcracking, since not every shielding event during the course of crack extension corresponds to an increase in the R-curve. Moreover, as seen in the composite cases, the local events leading to toughening behavior may not be associated with the microcracking even in the presence of a large population of microcracks.

Introduction

Fracture toughness of single phase brittle solids is much higher when they are in polycrystalline form in comparison to their single crystal form. In addition, in polycrystalline form the fracture toughness increases only over a discrete range of grain size; further increases in the grain size cause significant reductions in the measured toughness values (1-4). Apart from the energy expenditure due to the nucleation of microcracks (5) and their elastic interactions as summarized in ref. 6, other mechanisms such as crack pinning (7), crack bridging and pull-out by large grains (3, 8-10), and crack deflection and branching due to kinking (11), also have been suggested to explain the increase in the toughness with increasing grain size. The deterioration in the toughness with further increases in the grain size was attributed to mechanisms such as: the grain size dependency of dilatation originating from the residual stresses, an increase in the density of pre-existing microcracks due to the thermal cracking (12, 13) and microcrack coalescence resulting from extensive microcracking (11).

When these brittle solids are in the composite form reinforced either with fibers or with laminates the composite fracture toughness is significantly higher than the matrix toughness. Most of the mechanisms given above are also assumed to be responsible for this extra increase in the toughness; however, they are related to the reinforcing phase rather than the matrix. The contributions of each mechanism to the overall toughness have been suggested to be additive (10, 14). Although theoretical treatments of the role of reinforcement in the brittle solids are available (15-18), only a few consider the large scale matrix microcracking behavior. In the development of micromechanistic models to predict the toughening behavior, it is also important to note that apart from the influence of microstructural features there is a dependency of the measured fracture toughness values on the crack length (19) and the growth history (20).

In this study, a set of numerical analyses of crack growth was performed to elucidate the mechanism of microcracking on the fracture behavior of microcracking brittle solids and composites. The results obtained were compared with the available continuum description of microcracking.

Details of the FEM Analyses

In the present study two types of crack elements based on the hybrid technique (21), one for the microcracks and the other for the main crack, were employed and the details are given in (22). The effects of microcracking ahead of a growing main crack in plane-strain were analyzed as a boundary value problem for a circular region surrounding the crack tip. The outer boundary of this region is far enough away from the crack tip so that the elastic stress field on the boundary remains virtually unaffected by the microcracking. The FEM mesh used in the analyses is shown in Fig. 1. The dark areas in the bottom rectangular sector indicate the locations and distribution of the reinforcements in the simulated composite microstructure. The microcrack zone was developed only in the most inner rectangular region. The condition for microcrack nucleation within the each element was based on the attainment of a critical normal stress, σ_f, at a randomly pre-determined crack plane for that element. The mean value of σ_f and its selection criterion was based on the relationship (23)

$$K_{IC} = \sigma_f \sqrt{2\pi x_o} \quad (1)$$

where x_o is a length scale proportional to the microcrack size (3 to 5 times the microcrack size) and K_{IC} is the intrinsic fracture toughness of the matrix. Based on the strength results in (24, 25) it can be assumed further that :

$$\sigma_f = \left\{ \frac{4\,E\gamma}{\pi(1-\nu^2)c_o} \right\}^{\frac{1}{2}} \quad (2)$$

where E is the Young's modulus, υ is the Poisson's ratio, γ is the surface energy for crack nucleation and c_o is the length of the crack nucleating microstructural features (e.g., grain size or crack nucleating second phase particles). The fracture stress σ_f is also assumed to have a normal distribution with a standard deviation of

0.5.

The local stress intensity factor at the main crack tip K_{tip} was continuously calculated from the stiffness matrix formulation of the crack element for the main crack tip. The condition required for the main crack to propagate was the attainment of an intrinsic fracture toughness value K_{IC} at the crack tip (i.e. $K_{tip} \geq K_{IC}$). With the satisfaction of this criterion the crack was allowed to propagate one element by nodal release technique (boundary conditions for the nodes to be released at the crack tip were changed from normal displacement constraint to traction free condition). The finite element equations were then re-solved for the new condition. If the crack extension criterion was still fulfilled the propagation steps were repeated until the stress intensity factor at the main crack tip K_{tip} fell below the K_{IC} value. At this stage the outer displacements were increased for a new value of K_{app} and overshooting of the crack tip stress intensity factor was always prevented by taking very small displacement increments.

For each increment the applied stress intensity factor, K_{app}, was also calculated from the most outer ring of elements using

$$J = \int_{\Gamma} (U dy - T_i \frac{\partial u_i}{\partial x} ds) \qquad (3)$$

where U is the strain energy density, T_i is the traction vector, u_i is the displacement vector and ds is the arc length along the integration contour Γ. These calculated K_{app} values from the J-integral, together with stress intensity factor values K_{tip} evaluated for the main crack tip and the intrinsic fracture toughness K_{IC}, were used in the construction of shielding/amplification diagrams and crack growth resistance curves (R-curves) for advancing cracks.

Results

In order to establish the role of wake region on the shielding behavior the initial analyses were carried out for three cases with the pre-nucleated microcrack zones shown in Fig. 2. Since in the analyses the symmetry conditions were enforced, the microcracks were also symmetric along the crack plane. In the first case, the main crack propagates in an uncracked zone then enters into the microcrack zone and growth continues in this zone. In the second case, initial growth of the main crack occurs in a microcrack zone and subsequent propagation takes place in an uncracked zone. In the third case, simulation crack propagation occurs completely in a microcrack zone. However, for the last case, the microcracks were identical to those in the previous two cases and were created by basically joining the two zones together. For these cases the ratios of the K_{app} to K_{tip} are summarized with the normalized crack extensions in Fig. 3. In the figure the larger values of K_{app}/K_{tip} indicate increasing shielding effect and the opposite indicates the amplification due to microcracking. In the first case, main crack approaching the microcrack zone, the K_{app} and K_{tip} values were almost equal to each other (within 1%) until the main crack entered into the microcrack zone. This indicates the accuracy of the crack tip elements since K_{app} and K_{tip} values were evaluated independently and with two completely different schemes. As the main crack propagated in the microcrack zone the ratio of K_{app}/K_{tip} became gradually greater than unity indicating a general shielding behavior. However, this increase was not smooth and several amplifications of K_{tip} from the current value can be seen. In the second case, main crack leaving the microcrack zone, due to the pre-existing wake region (Fig. 2b) and also due to the immediate interactions with microcracks, the shielding was immediate in comparison to the first case. During the crack extension in the microcrack zone several shielding/amplification events took place. In this case the most important result is that the shielding behavior remained in effect after the microcrack zone had been left behind at a significant distance from the current crack tip. In the third case where the microcrack locations were the same as in two previous cases, it is particularly interesting to note that shielding/amplification events during the first portion of the crack growth are almost identical to the second case. This indicates that the extent of the microcrack zone ahead of the crack tip does not have a significant effect on the shielding/amplification behavior. Subsequently, as the crack extended into the second half of the microcrack zone, the shielding/amplification events again occurred in the same main crack tip locations as in the first case.

The R-curve behavior (K_{app} normalized with the intrinsic fracture toughness K_{IC}) resulting from these simulations is shown in Fig. 4. The flat regions in these curves represent the condition where K_{tip} stress intensity factor was either equal to or greater than the K_{IC} and increases correspond to the condition where K_{tip} was smaller than the K_{IC}, hence the K_{app} had to be increased to maintain the crack propagation. From Figs. 4 and 5 the role of wake region, the history dependency and including the amount of crack extension on the toughening characteristics can be seen. In the first case, the R-curve remained flat due to lack of any shielding until the main crack entered into the microcrack zone. The overall increase in the toughness was greater for the last case. This is due in part to development of a larger wake region and also in part to more interactions with microcracks which favors shielding with increasing crack length. However, these effects will eventually reach a level such that the increase in the toughening reaches to a limiting value. This can be seen particularly when comparing the last elevations in the toughness values between the first and the third cases.

The effects of continuous nucleation on the crack growth behavior in an unreinforced matrix and the role of reinforcement on the crack growth behavior of microcracking composites were investigated for the reinforcement distribution shown in the rectangular sector at the bottom of Fig. 1. The volume fraction of the reinforcement was about 19%; however, since the analyses were carried out in two dimensions, they were continuous in the thickness direction. The reinforcements were also assumed to fail and generate microcracks. Their fracture strength for the microcrack nucleation was assumed to be the same as that of the matrix in eq. 1, with similar strength distribution. It was further assumed that the reinforcing phases have the same intrinsic fracture toughness K_{IC} as the matrix; therefore, the same crack propagation criterion was applied when the main crack was crossing the reinforcements. Two simulations were carried out with Young's modulus ratio of reinforcing phase to matrix (E_f/E_m) of 2.0 and 0.5. The evolution of the damage and microcrack zone developments in the composites were compared with the matrix damage formation in Fig. 5. In this figure, first crack length corresponds to the condition where initial main cracks were ready to propagate (i.e., $K_{tip} \geq K_{IC}$). For the composite having higher modulus ratio the location of the column of microcrack formation ahead of the main crack tip corresponds to the location of the nearest reinforcement. This behavior is associated with the development of higher stresses in the reinforcements in this composite system. On the other hand, the initial damage in the composite with low modulus ratio was similar to the one in the matrix alone. At final crack lengths, although zone widths appear to be similar in both composites, the number of nucleated microcracks is much larger for the low modulus case. The variations in the K_{app}/K_{tip} values and R-curves were compared with the data obtained for the matrix in Figs. 6 and 7 respectively. At the very initial stages of the crack growth the shielding/amplification events in both composites and in the matrix were similar. However, as soon as the main crack encountered the first reinforcement, shielding/amplification characteristics deviated from each other considerably. In the case of high modulus ratio there was a large amplification in the K_{app}/K_{tip} ratio, whereas in the case of low modulus ratio there was a large shielding. As can be seen from the figure, this behavior was repeated periodically each time the main crack crossed the reinforcing phase. This initial shielding was so large for the low modulus ratio that K_{app} had to be

increased considerably as can be seen from the R-curve. The large scale microcracking with later crack advances in this composite, therefore, is associated with this large elevation of the K_{app}. Although a large scale microcracking occurred for this case, the increases in the R-curve correspond to the locations where the main crack was crossing the reinforcements. Similarly, in the composite with high modulus ratio, the elevations in the R-curve took place just prior to the main crack encountering the reinforcements.

Discussion

The suggested theoretical analyses of the toughening behavior resulting from the microcracking usually contains two components: the elastic interactions of the microcracks, and a dilatational component arising from the residual stresses. The latter contribution is not included in the analyses presented in this study. On the other hand, the random orientation and nucleation of the microcracks at all locations above the crack plane were provided in the analysis. Therefore, the results presented pertain to the elastic interaction component. However, a good understanding of this component may lead to development of more realistic and accurate micromechanistic models, since these two components could be of the same order of magnitude in their contributions to toughening as reported in (11). As given in the introduction section, several observations were made regarding the characteristics of microcracking zone in simulations using discrete microcrack models. One of them of interest was that the microcracks in the wake region have little or no effect on the toughening mechanism by shielding (5). The results obtained in this study, Figs. 3 and 4, clearly exhibit the role of the wake region on the toughening behavior in agreement with the experimental results (26).

In the present study, a critical value of normal stress, σ_f, acting on the microcrack plane was chosen as the microcrack nucleation criterion which can be related to the size of microcrack nucleating microstructural features (grain size or second phase particles) and also can be related to the intrinsic fracture toughness K_{IC} of the material through eqs. 1-2. Of course the other stress components, such as mean stress as in (27), can also be selected; however, in this study no attempt was made to investigate the role of other nucleation criteria on the microcracking behavior.

The role of continuous microcrack nucleation on the crack growth behavior in the matrix material and in the composites were studied for two reinforcement types having rigid interfaces. In these simulations, the reinforcements were also assumed to fail and generate microcracks with the same criterion used for the matrix. It was further assumed that the reinforcing phases have the same intrinsic fracture toughness K_{IC} as the matrix; therefore, the same crack propagation criterion was applied when the main crack was crossing the reinforcements. For both types of reinforcements, the overall number of microcracks generated and the extent of the microcrack zones were much larger than the matrix, Fig. 5. However, as can be seen from the shielding and amplification diagrams and the evolution of the R-curves, Figs. 6 and 7, the mechanism of toughening appears to be associated with the interactions of the main crack tip with the stress fields created by the reinforcements, rather than the elastic interactions of the microcracks with the main crack.

Based on path independence of the J-integral within the microcrack zone and outside the microcrack zone, several continuum solutions to estimate the magnitude of the shielding behavior in isotropic microcracking and anisotropic microcracking cases have been provided (28-31). For isotropic microcracking the magnitude of shielding is given as (28)

$$\frac{K_{app}}{K_{tip}} = \left\{ \frac{1.0 - \upsilon_1^2 E}{1.0 - \upsilon^2 E_1} \right\}^{\frac{1}{2}} \qquad (4)$$

and

$$\frac{E_1}{E} = 1 - \frac{16}{45} \frac{(1-\upsilon^2)(20-3\upsilon)}{(2-\upsilon)} \beta \qquad (5)$$

where E_1 and υ_1 are Young's modulus and Poisson's ratio of the microcrack saturation condition and E and υ are Young's modulus and Poisson's ratio for the uncracked condition. ß is the non-dimensional microcrack density and for randomly oriented through cracks is taken as Na^2l, where N is the number of microcracks per unit volume, a is the microcrack length and l is the crack depth (29). The magnitude of shielding resulting from isotropic cracking under normal stress for steadily growing cracks is given as (27)

$$\frac{K_{tip}}{K_{app}} = 1 - 1.471\beta. \qquad (6)$$

By taking υ=0.3 in eq. 5, for the microcrack densities in this study, the predicted shielding behaviors from eqs. 4 and 5 are compared with the value obtained from the FEM solutions in Fig. 8. In this figure, the points are the mean value and error bars indicate the maximum and minimum observed values during the course of the crack extension in the FEM analyses. Although the scatter is large, the predicted shielding behaviors from the continuum description of microcracking are generally in agreement with the observed values. However, in this correlation several aspects should be considered. In the continuum description, when shielding behavior is considered due to elastic interactions alone, the microcrack zone size and the extent of the wake region with crack advance do not appear as contributing parameters in the formulation. All of these parameters have an apparent effect on the shielding behavior as seen from Figs. 2-4. For continuous microcrack nucleation cases, the predicted shielding values from eq. 6 are compared with the values observed from FEM analyses in Fig. 9. As can be seen, the correlation is particularly good for the matrix case alone; however, as seen in the composite cases, the local events leading to toughening behavior may not be associated with microcracking even in the presence of a large population of microcracks. Although such models closely predict the magnitude of shielding, they do not resolve the details of the micromechanism of toughening as seen in this study, as also indicated in (5).

Conclusions

In this study, the role of continuous microcrack nucleation on the crack growth behavior in brittle microcracking solids and composites were numerically investigated. The results obtained from the finite element analysis are compared with the continuum description of the microcracking. Although continuum description can provide a reasonable estimation of shielding, it fails to resolve the details of micromechanism of toughening resulting from microcracking, since not every shielding event during the course of crack extension corresponds to an increase in the R-curve. Moreover, as seen in the composite cases, the local events leading to toughening behavior may not be associated with the microcracking even in the presence of a large population of microcracks.

Acknowledgements

This work was performed for the United States Department of Energy by Iowa State University under contract No. W-7405-Eng-

82. This research supported by the Director of Energy Research, Office of Basic Energy Sciences.

References

1. R. W. Rice, S. W. Freiman and P. F. Becher, J. Am. Ceram. Soc., 64 (1981), 345.

2. P. L. Swanson, C. J. Fairbanks, B. R. Lawn and Y. W. Mai, J. Am. Ceram. Soc., 70 (1987), 279.

3. G. Vekinis, M. F. Ashby and P. W. R. Beaumont, Acta Metall. Mater., 38 (1990), 1151.

4. R. Steinbrech, R. Knehens and W. Schaarwachter, J. Mater. Sci., 18 (1983),265.

5. M. Kackanov, E. L. E. Montagut and J. P. Lawres, Mech. Mater., 10 (1990), 59.

6. S. B. Biner, Acta Metall. Mater., (in press).

7. F. F. Lange, Philos. Mag., 22 (1970), 983.

8. Y. W. Mai and B. R. Lawn, J. Am. Ceram. Soc., 70 (1987), 289.

9. S. T. Bennison and B. R. Lawn, Acta Metall. Mater., 37 (1989), 2859.

10. P. F. Becher, J. Am. Ceram. Soc., 74 (1991), 255.

11. L. X. Han, R. Warren and S. Suresh, Acta Metall. Mater., 40 (1992), 259.

12. Y. Fu and A. G. Evans, Acta Metall. Mater., 30 (1982), 1619.

13. A. G. Evans and Y. Fu, Acta Metall. Mater., 33 (1985), 1525.

14. M. Ruhle, A. G. Evans, R. M. McMeeking, P. G. Chamralambides and J. W. Hutchinson, Acta Metall. Mater., 35 (1987), 2701.

15. D. B. Marshall and B. N. Cox, Acta Metall. Mater., 33 (1985), 2013.

16. A. G. Evans and D. B. Marshall, Acta Metall. Mater., 37 (1989), 2567.

17. M. D. Thoules and A. G. Evans, Acta Metall. Mater., 36 (1988), 517.

18. A. G. Evans, Mat. Sci. Eng., A143 (1991), 63.

19. F. W. Zok and C. L. Hom, Acta Metall. Mater., 38 (1990), 1895.

20. R. Knehens and R. Steinbreck, J. Mater. Sci. Lett., 1 (1982), 327.

21. P. Tong, T. H. H. Pian and S. J. Lasry, Int. J. Num. Meth. Engng., 7 (1973), 297.

22. S. B. Biner, Eng. Fract. Mech., (submitted).

23. A. A. Griffith, Phil. Trans. Roy. Soc. London, A221 (1921), 163.

24. F. J. P. Clarke, Acta Metall. Mater., 12 (1964), 139.

25. S. C. Carniglia, J. Am. Ceram. Soc., 55 (1972), 243.

26. R. Knehens and R. Steinbreck, J. Mater. Sci. Lett., 1 (1982), 327.

27. J. W. Hutchinson, Acta Metall. Mater., 35 (1987), 1605.

28. B. Budiansky and R. J. O'Connell, Int. J. Solids and Struct., 12 (1975), 81.

29. N. Laws and J. R. Brockenbrough, Int. J. Solids and Struct., 23 (1987), 1247.

30. A. G. Evans and K. T. Faber, J. Amer. Ceram. Soc., 67 (1984), 255.

31. P. G. Charambides and R. M. McMeeking, Mech. Mater., 6 (1987), 71.

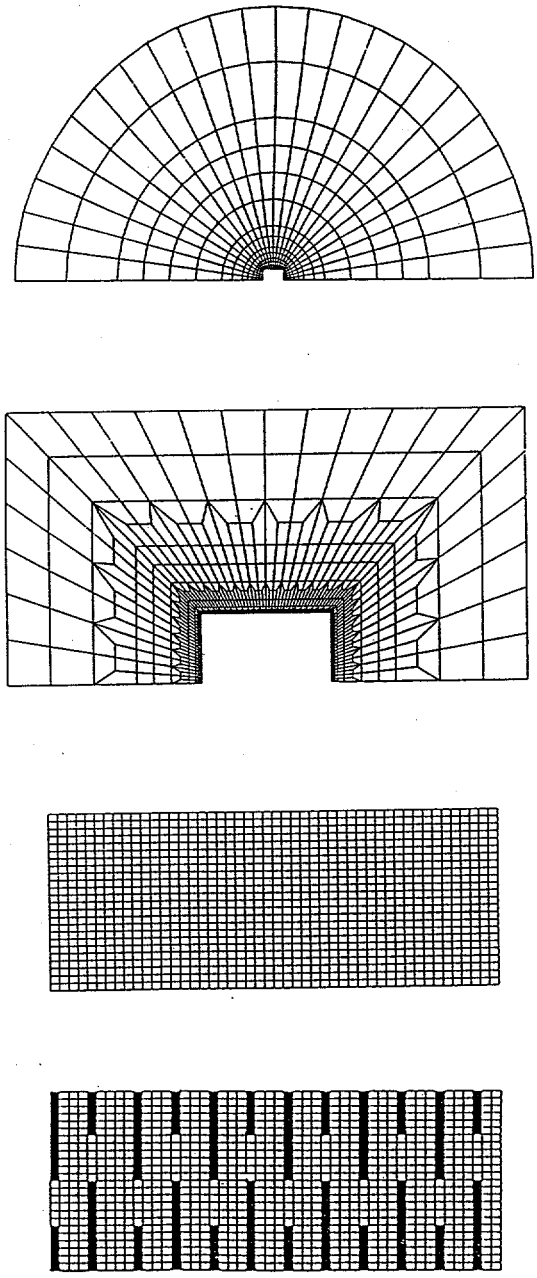

Figure 1: The FEM mesh used in the analyses. The dark areas in the bottom rectangular sector indicate the locations and distribution of the reinforcements in the simulated composite microstructure.

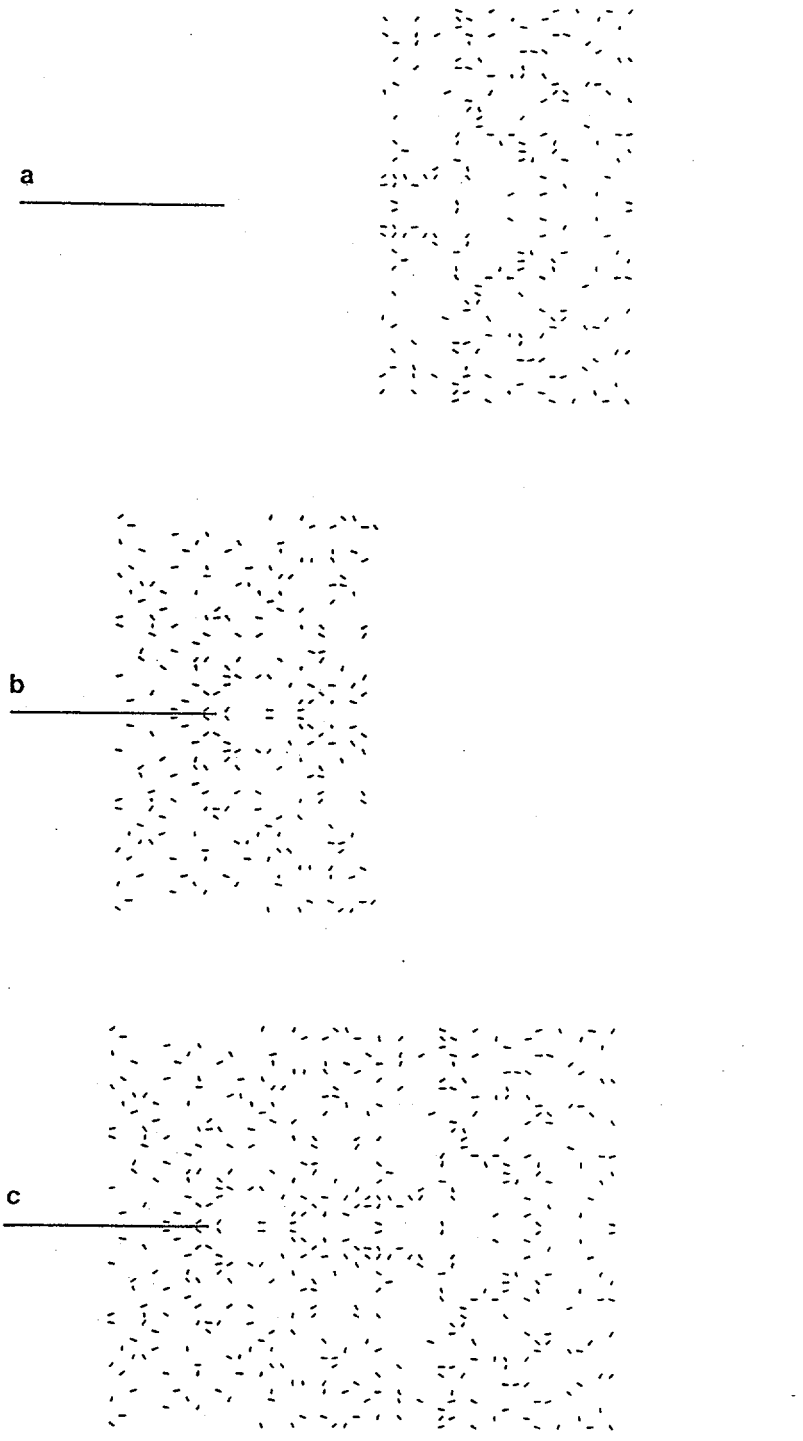

Figure 2: Microcrack zones and distribution of the microcracks used in the analyses for the role of wake region on the crack growth behavior. a) The main crack approaching to the microcrack zone and subsequent growth occurs in the microcrack zone. b) The initial growth of the main crack occurs in the microcrack zone and growth continuous in the uncracked zone. c) Main crack propagation completely occurs in the microcrack zone.

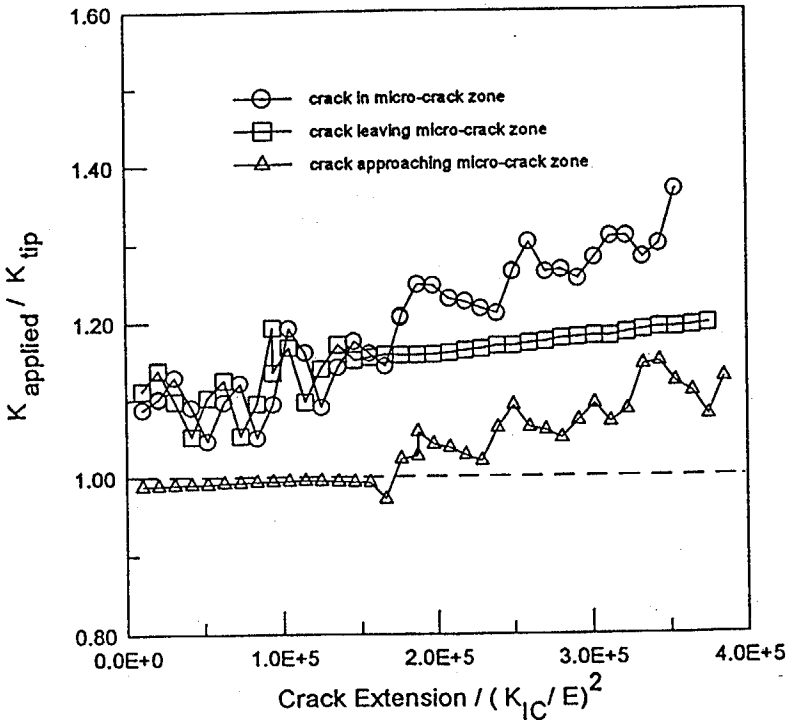

Figure 3: Shielding/amplification diagram for growing cracks in different microcrack zone lengths.

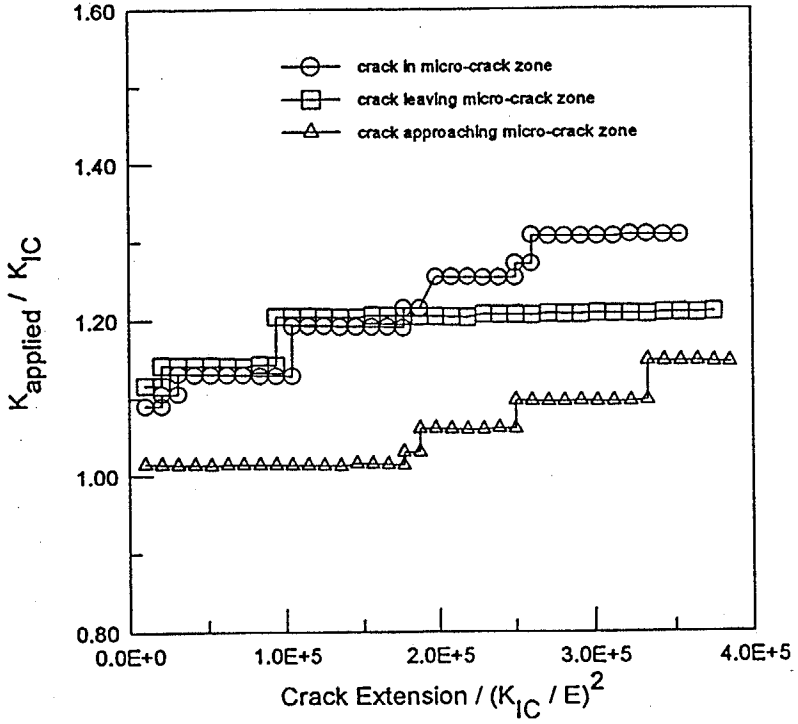

Figure 4: R-curve behavior for growing cracks in different microcrack zone lengths.

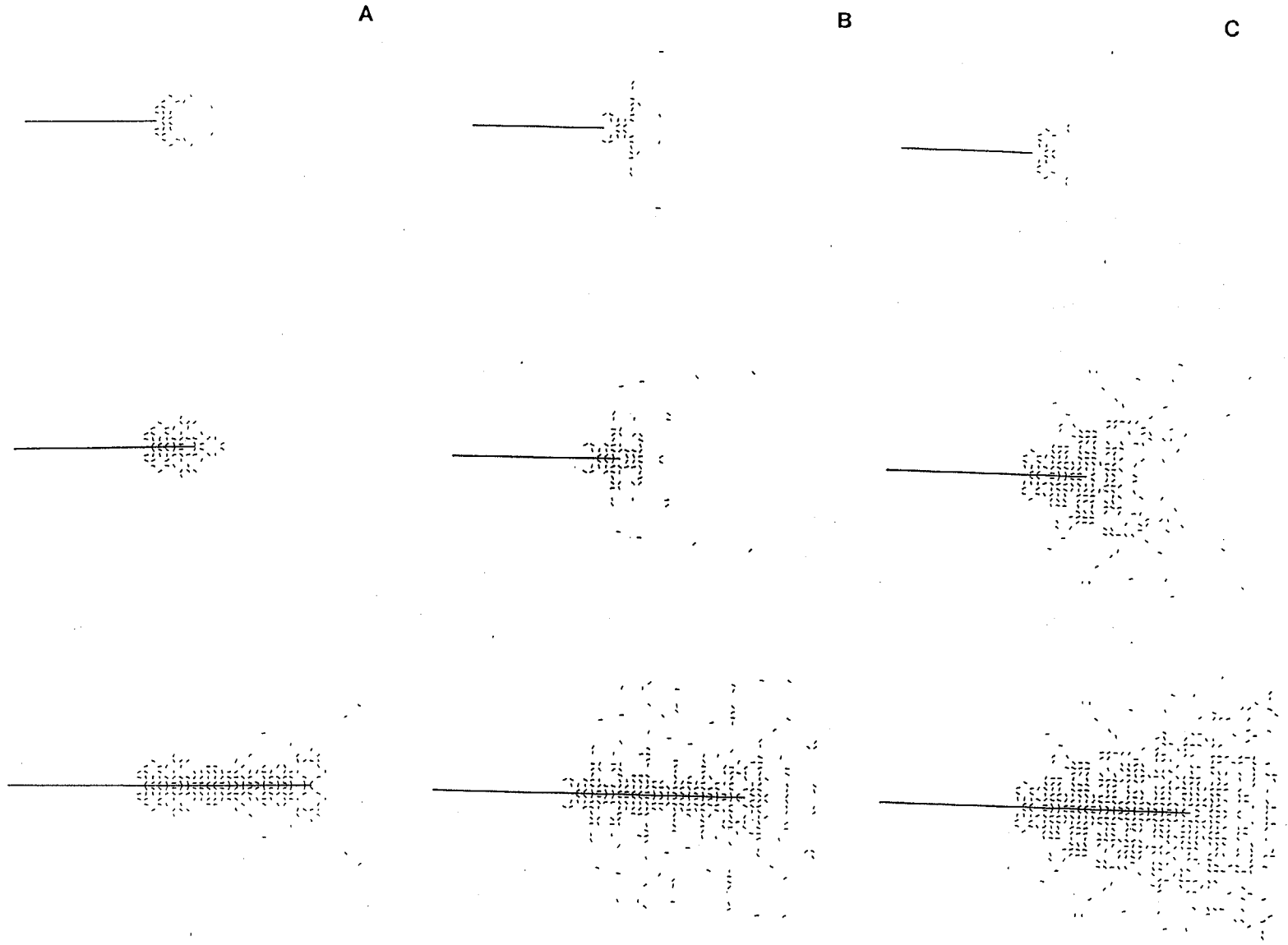

Figure 5: Development of the microcrack zones with crack growth. a)- Matrix, b)- Composite with E_f/E_m of 2.0 and c)- Composite with E_f/E_m of 0.5.

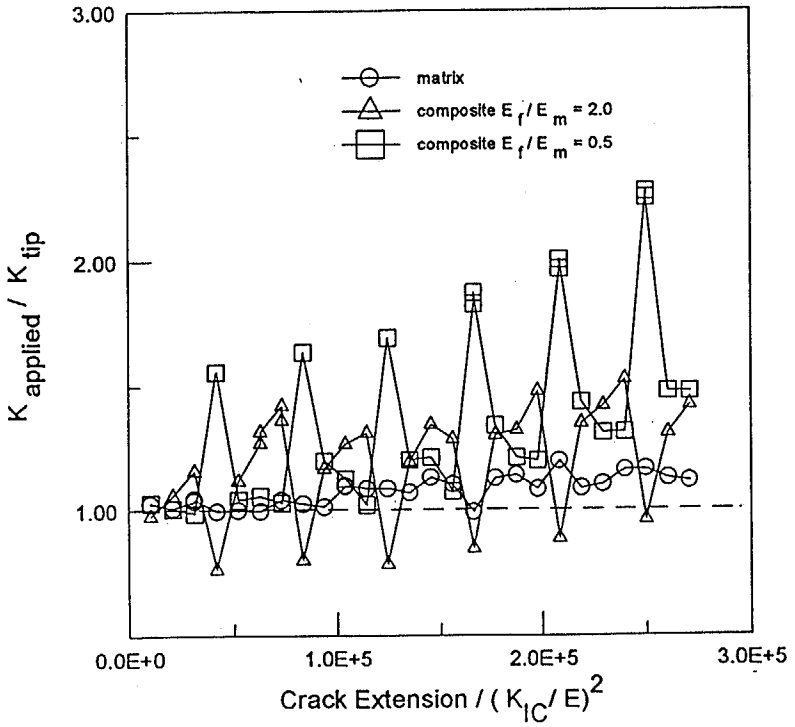

Figure 6: Variation in the shielding/amplification behavior with crack growth in the matrix and in the composites.

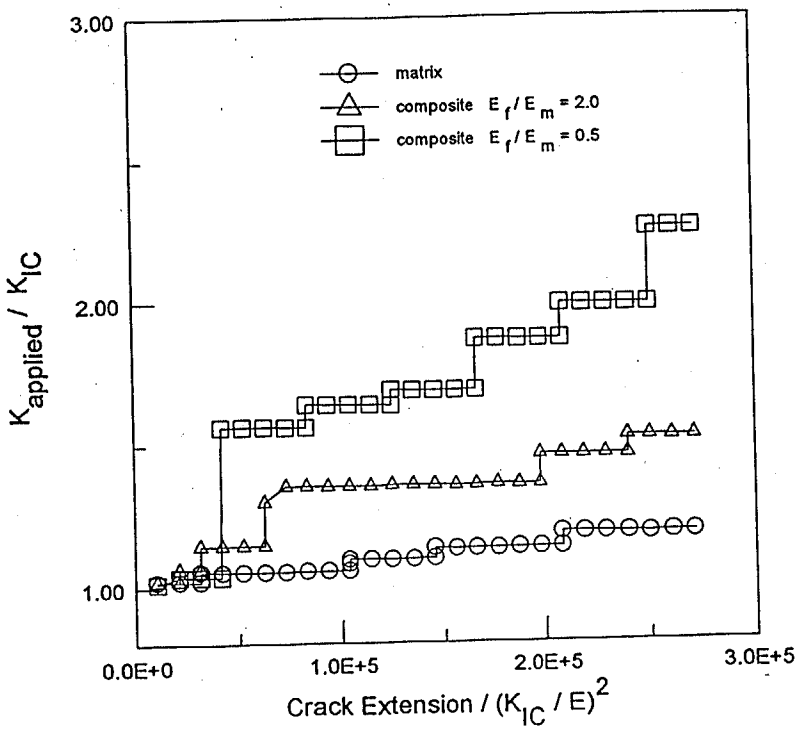

Figure 7: R-curve behavior of the matrix and the composites.

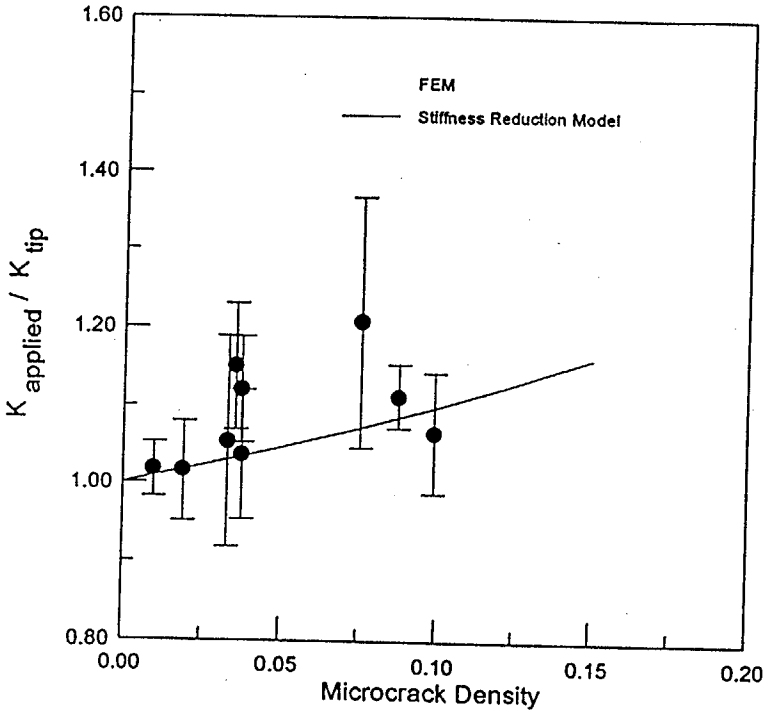

Figure 8: Comparison between the analytically calculated shielding behavior and the results obtained from the FEM analysis for pre-nucleated crack cases.

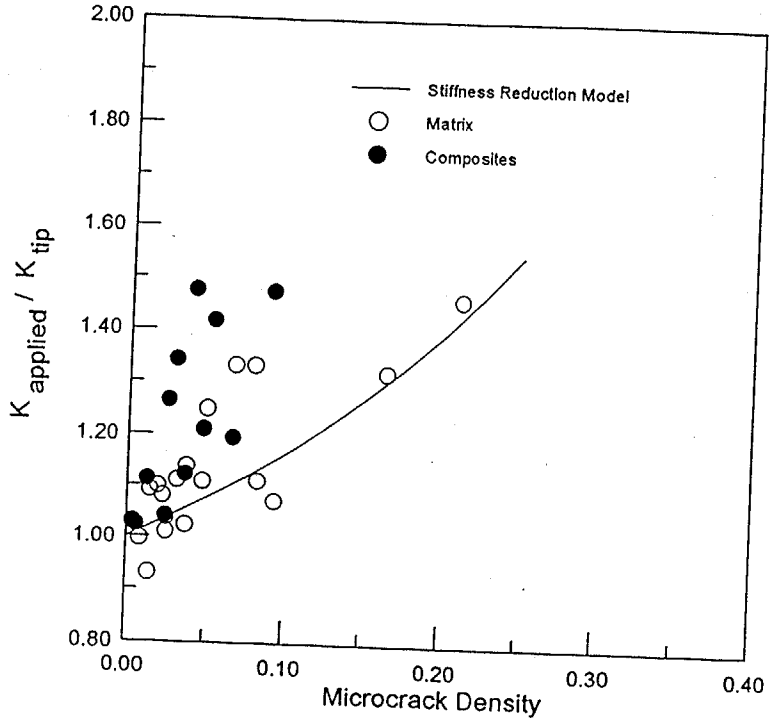

Figure 9: Comparison between the analytically calculated shielding and the data obtained from the FEM analysis for continuous microcrack nucleation cases.